MAMMOGRAM ENHANCEMENT USING A CLASS OF SMOOTH WAVELET

Zhuoer Shi, DeSheng Zhang, Haixiang Wang, Donald J. Kouri

Department of Physics and Chemistry
University of Houston, Houston, TX 77204, USA

David K. Hoffman

Ames Laboratory and Department of Chemistry
Iowa State University, Ames, IA 50011, USA

ABSTRACT

We proposes an mammogram enhancement technique using interpolating distributed approximating functional (DAF) wavelets, visual group normalization (VGN), softer logic masking (SLM) filtering, and nonlinear sharpening enhancement (ESE) techniques. These are formulated to normalize the wavelet coefficients, remove perceptual redundancy and obtain optimal visualization of the important diagnostic features for digital mammograms.

1. INTRODUCTION

Distributed approximating functionals (DAFs) are generated by Gaussian-modulated Sinc, Hermit, or Lagrange functionals. Such DAFs are smooth and decaying in both time and frequency representations and have been used for numerically solving various linear and nonlinear partial differential equations with extremely high accuracy. Examples include DAF-simulations of 3-D reactive quantum scattering, the Kuramoto-Sivashinsky equations describing flow pattern dynamics for a circular domain, the sine-Gordon equation near homoclinic orbits, and a 2-D Navier-Stokes equation with non-periodic boundary conditions [1].

In this paper, the Sinc-DAF is employed to construct a new class of interpolating wavelets and specifically for use in mammogram enhancement. Human visual sensitivity is utilized to construct the *visual group normalization* (VGN) technique, which is used to re-scale the wavelet decomposition coefficients for perceptual adapted reconstruction. A nonlinear contrast stretch and enhancement functional is realized for wavelet-based multi-scale gradient transformation and feature-sensitive image reconstruction, which enables us to obtain accurate space-localization of the important features of the mammogram. The combined techniques can greatly improve the visualization of low-contrast components, which is important for diagnosis. Additionally, the DAF-wavelet image processing can be implemented using the interpolation technique that implies the extreme efficiency for fast implementation.

2. GENERALIZED SINC WAVELETS

2.1 Sinc Wavelet

The π band-limited Sinc function,

$$\phi(x)=\sin(\pi x)/(\pi x)\in C^{\infty} \tag{1}$$

constructs the interpolation in *Paley-Wiene*r space. Every π band-limited function $f\in L^2(R)$ can be reconstructed by the equation

$$f(x)=\sum_k f(k)\frac{\sin\pi(x-k)}{\pi(x-k)} \tag{2}$$

The associated wavelet function—Sinclet is defined as (as shown in Fig.1)

$$\psi(x)=\frac{\sin\pi(2x-1)-\sin\pi(x-1/2)}{\pi(x-1/2)} \tag{3}$$

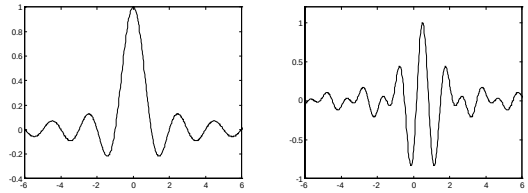

(a) (b)

Figure 1. π band-limited interpolating wavelets. (a) *Sinc* function, (b) *Sinclet* wavelet.

The scaling function is the well-known ideal low-pass filter which possesses the filter response

$$H(\omega)=\begin{cases}1, & |\omega|\pi/2\\ 0, & \pi/2<|\omega|\le\pi\end{cases} \tag{4}$$

Its impulse response can be described as

$$h[k]=\frac{1}{2\pi}\int_{-\pi/2}^{\pi/2}e^{jk\omega}d\omega=sin(\pi k/2)/(\pi k) \tag{5}$$

The so-called half-band filter [2] only possesses non-zero impulses at odd integer samples, $h(2k+1)$, while at even integers, $h[2k]=0$, except for $k=0$.

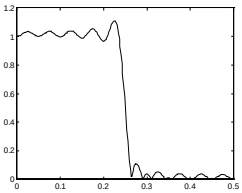

Figure 2. Gibbs overshot of Sinc FIR implementation.

However, this ideal low-pass filter can not be implemented physically. Because the digital filter is an IIR (infinite impulse response) solution, its digital cutoff FIR (finite impulse response) implementation introduces Gibbs phenomenon (overshot effect) in Fourier space, which degrades the frequency resolution (Fig.2). The explicit compactly supported Sinc scaling function and wavelet, as well as their dual scaling function and wavelet, are shown in Fig.3. We find that the cutoff Sinc has decreased regularity, which is manifested by a fractal-like behavior and implies poor time localization.

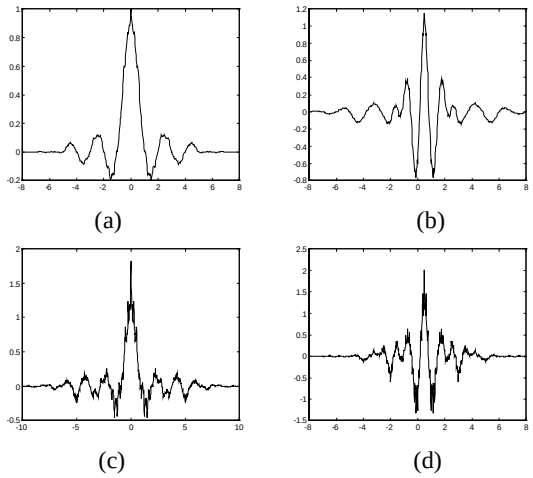

(a) (b) (c) (d)

Figure 3. Sinc cutoff wavelets (M=9). (a) Scaling, (b) wavelet, (c) dual scaling, (d) dual wavelet.

2.2 Gaussian-Sinc DAF Wavelets

Because the ideal low-pass Sinc wavelet can not be implemented "ideally" by FIR filters, a windowed weighting technique is introduced here to eliminate the cutoff singularity, and improve the time-frequency localization. We choose sinc-DAF [3] to construct interpolating scalings,

$$\phi(x) = W_\sigma(x)\frac{\sin(\pi x/2)}{\pi x} \tag{6}$$

where $W_\sigma(x)$ is a window function which is selected as a Gaussian,

$$W_\sigma(x) = e^{-x^2/2\sigma^2}. \tag{7}$$

It satisfies the minimum frame bound condition in quantum physics and improves the time-frequency resolution. Here σ is a window width parameter, and $P(x)$ is the Sinc interpolation kernel. The Gaussian window in our DAF-wavelets efficiently smoothes out the Gibbs oscillations, which plague most conventional wavelet bases. The following equation shows the connection between the B-spline function and the Gaussian window [4]:

$$\beta^N(x) \cong \sqrt{\frac{6}{\pi(N+1)}}\exp\left(\frac{-6x^2}{N+1}\right) \tag{8}$$

for large N. As in Fig. 6, if we choose the window width

$$\sigma = \eta\sqrt{(N+1)/12} \tag{9}$$

the Gaussian window can be regarded as a fine estimation of the B-spline function. The cascade smooth construction of DAF-wavelets using lifting schemes [5] are shown in Fig.4. The associated frequency responses of the subband filters are shown in Fig.5 with fine frequecny resolution.

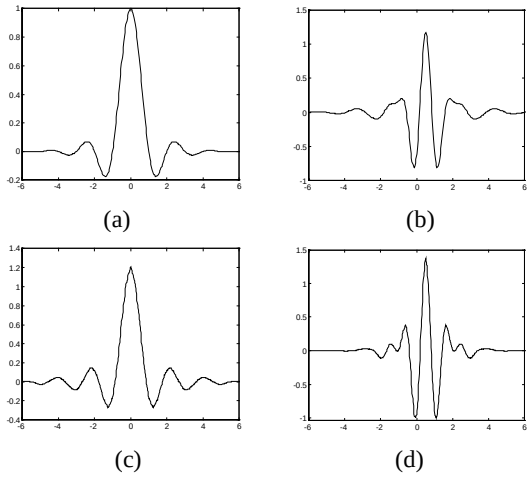

(a) (b) (c) (d)

Figure 4. DAF wavelets (N=5, η=3). (a) Scaling, (b) wavelet, (c) dual scaling, (d) dual wavelet.

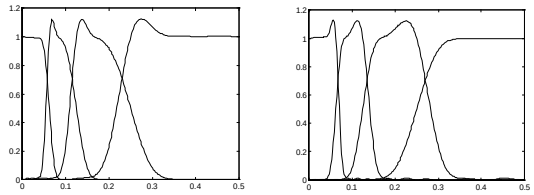

(a) (b)

Figure 5. Frequency response of equivalent filters (N=5, η=3). (a) Decomposition, (b) reconstruction.

3. VISUAL GROUP NORMALIZATION

3.1 Magnitude Normalization

At each decomposition level, 2D wavelet coefficients are divided into four sub-blocks, *LL*, *HL*, *LH*, and *HH*. *L* and *H* represent the low-pass and high-pass subband filtering results, respectively. *HL* means the output of signal passing the horizontal high-pass filter and vertical low-pass filter. The sub-

block coefficients *HL*, *LH* and *HH* represent the multiscale difference operation in different spatial directions, horizontal, vertical, and diagonal, respectively. At each level of analysis, the bandwidth of the equivalent subband filters decreases by a factor of two [6].

Wavelet coefficients can be regarded as the output of the signal passing through *equivalent decomposition filters* (EDF). The responses of the EDF are the different combination of subband filters and down-sampling operations. The EDF responses determine the magnitude distribution of the decomposition coefficients. To adjust the magnitude response in each block, the decomposition coefficients $C_{j,m}(k)$ in block (j,m) are normalized with a magnitude factor $\lambda_{j,m}$. Here j represents the decomposition layer, and m denotes the different orientation block (*LL*, *LH*, *HL* or *HH*). The normalizing factor is designed as the reciprocal of the maximum magnitude of the EDF response.

$$\lambda_{j,m} = \frac{1}{\sup_{\omega\in\Omega}\{|LC_{j,m}(\omega)|\}}, \quad \Omega=[0,2\pi] \tag{10}$$

The magnitude normalized coefficients $NC_{j,m}(k)$ are defined as

$$NC_{j,m}(k)=\lambda_{j,m}C_{j,m}(k). \tag{11}$$

This idea was recently extended to Group Normalization (GN) of wavelet packets for signal processing and was shown to yield the optimal performance [7].

3.2 Perceptual Luminance Normalization

The visibility of wavelet transform coefficients will depend on the display visual resolution in pixel/degree. Given a viewing distance V in inches and a display resolution d in pixel/inch, the effective display visual resolution (DVR) R is

$$R=dV\tan(\pi/180)\approx dV/57.3 \tag{12}$$

The visual resolution is the viewing distance (dV) divided by 57.3. When the decomposition layer increases, the bandwidth of the EDF decreases by a factor of two while the frequency resolution doubles. Correspondingly, the space resolution (display resolution) decreases by a factor of two. Each sub-block of wavelet coefficients corresponds to a spatial-frequency band. For a display resolution of R pixel/degree, the spatial frequency f of level j is

$$f=2^{-j}R \tag{13}$$

For gray-scale mammogram image, the just-noticeable quantization threshold of Y is generally different at each spatial frequency. The contrast sensitivity declines when the spatial frequency increases (whereas, the size of the stimuli decreases). This fact of visual response is used to construct the "perceptual normalization" that enables efficient removal of the visual redundancy with respect to the perceptual importance. A simple nonlinear model of different frequency bands has been presented in [8], which can be used to construct the "perceptual normalization" response magnitude $Y_{j,m}$ in luminance spaces. We extend the definition as

$$Y_{j,m} = a10^{k\left(\log\frac{2^j f_0 d_m}{R}\right)^2} \tag{14}$$

where a defines the minimum threshold, k is a constant, R is the *display visual resolution* (DVR), f_0 is the spatial frequency, and d_m is the directional response factor.

3.3 Contrast Sensitivity Normalization

Visual sensitivity is defined as the inverse of the contrast to produce a threshold response [9],

$$S=1/C, \tag{15}$$

where C is generally referred to simply as the threshold. The Michelson definition of contrast,

$$C=(L_{max}-L_{mean})/L_{mean} \tag{16}$$

is used, where L_{max} and L_{mean} refer to the maximum and mean luminances of the waveform in a luminance channel. The variations in sensitivity as a function of light level are primarily due to the light-adaptive properties of the retina and are referred to as the *amplitude nonlinearity* of the HVS. The variations as a function of spatial frequency are due to the optics of the eye combined with the neural circuitry; these combined effects are referred to as the *contrast sensitivity function* (CSF). Combining the perceptual lossless normalization, the visual sensitivity normalization and the magnitude normalized factor $\lambda_{j,m}$, we obtain the combined normalization matrix $Q_{j,m}$

$$Q_{j,m}=2CY_{j,m}/\lambda_{j,m} \tag{17}$$

This treatment provides a human-vision-based normalization technique for the restoration of the important perceptual information. We denote the combination of the above-mentioned techniques the *Visual Group Normalization* (VGN).

4. IMAGE PROCESSING

For grayscale image contrast stretching, the objective is to improve the perception capability for image components that the human visual system is initially insensitive but is important for diagnosis. In other words, mammogram enhancement increases the cancer detection probability and precision. We first appropriately normalize the decomposition coefficients according to the length scale of the display device so that they fall within the interval of the device frame. Assume that the coefficients have already been properly adjusted using VGN so that the amplitude value $NC_{j,m}(k)$ falls into the dynamic range of the display device:

$$d_{\min} \le NC_{j,m}(k) \le d_{\max} \tag{18}$$

Without loss of generality, we consider the normalized gradient

$$U_{j,m}(k)=NC_{j,m}(k)/(d_{\max}-d_{\min}) \tag{19}$$

Wavelet analysis provides a natural characterization for multiscale image edges and can be easily extracted by various differentiations. Their idea was extended by Laine et al [10] to develop directional edge parameters based on a subspace energy measurement. Our starting point is to define an enhancement functional $E_{j,m}$

$$E_{j,m}=\alpha_{j,m}+\beta_{j,m}\Delta, \tag{20}$$

where Δ is the Laplacian and $-1\le\alpha_{j,m}, \beta_{j,m}\le 1$. The coefficients $\alpha_{j,m}$, $\beta_{j,m}$ can be easily chosen so that desired image features are emphasized. In particular we can emphasize an image edge of selected grain size. We note that a slight modification of $\alpha_{j,m}$ and $\beta_{j,m}$ results in orientation selected image enhancement.

Contrast stretching is an old but quite efficient method for feature selective image display. Lu and coworkers [11] have designed a hyperbolic function

$$g_j(k)=[\tanh(ak-b)+\tanh(b)]/[\tanh(a-b)+\tanh(b)] \tag{21}$$

for multiscale gradient transformation.

5. ENHANCEMENT RESULT

Mammograms are complex in appearance and signs of early disease are often small and/or subtle. The original MIAS image [12] is chopped at 768×800 size as shown in Fig. 6(a). The methods in chapter 4 are combined for enhancement processing. As shown in Fig. 6(b), there is a significant improvement in both edge representation and image contrast resulting from DAF-wavelet-based VGN and non-linear enhancement techniques. In particular, the domain and internal structure of higher-density cancer tissues are clearly displayed.

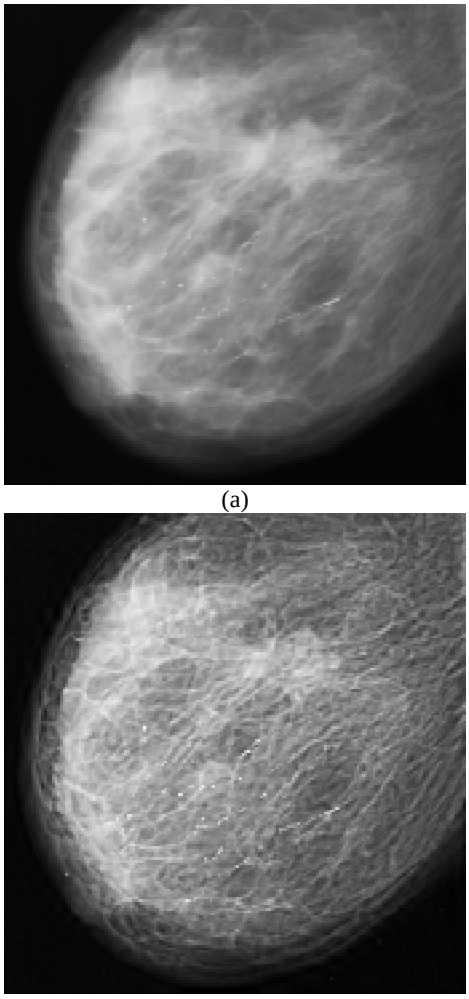

(a)

(b)

Figure 6. Mammogram enhancement. (a) Original mammogram, (b) enhancement result.

6. SUMMARY

The newly developed image enhancement techniques improve the imaging performance for earlier detection of cancer and malignant tumors. It improves the spatio-temporal resolution of biomedical images and enhances the visualization of the perceptually less-sensitive components that are very important for diagnosis. The method presented can be applied to various types of medical images. These include various X-ray images, mammography, magnetic resonance imaging (MRI), supersonic imaging, etc.

7. REFERENCES

[1] D. K. Hoffman, N. Nayar, O. A. Sharafeddin, and D. J. Kouri, "Analytic banded approximation for the discretized free propagator," *J. Physical Chemistry*, vol.95, no.21, pp.8299-8305, 1991.

[2] R. Ansari, C. Guillemot, and J. F. Kaiser, "Wavelet construction using Lagrange halfband filters," *IEEE Trans. CAS*, vol.38, no.9, pp.1116-1118, 1991.

[3] D. K. Hoffman, G. W. Wei, D. S. Zhang, and D. J. Kouri, "Shannon-Gabor wavelet distributed approximating functional," *Chem. Phys. Letters*, Vol. 287, pp. 119-124, 1998.

[4] M. Unser, A. Aldroubi, "Polynomial splines and wavelets-a signal processing perspective," *Wavelets-A Tutorial in Theory and Applications*, C. K. Chui (ed.), pp.91-122, Academic Press, 1992.

[5] W. Swelden, "The lifting scheme: a custom-design construction of biorthogonal wavelets," *Appl. And Comput. Harmonic Anal.*, vol.3, no.2, pp.186~200, 1996.

[6] M. Vetterli, C. Herley, "Wavelet and filter banks: theory and design," IEEE Trans. SP, Vol. 40, No. 9, pp.2207-2232, September 1992.

[7] Z. Shi, Z. Bao, "Group-normalized wavelet packet signal processing", *Wavelet Application IV*, SPIE, vol. 3078, pp.226~239, 1997.

[8] A. B. Watson, G. Y. Yang, J. A. Solomon, and J. Villasenor, "Visibility of wavelet quantization noise," *IEEE Trans. Image Processing*, vol. 6, pp. 1164-1175, 1997.

[9] N. Jayant, J. Johnston, and R. Safranek, "Signal compression based on models of human perception", *Proceedings IEEE*, vol.81, no.10, pp.1385~1422, 1993.

[10] A. F. Laine, S. Schuler, J. Fan and W. Huda, "Mammographic feature enhancement by multiscale analysis," IEEE Trans. MI, vol.13, pp.725-740, 1994.

[11] J. Lu, D. M. Healy Jr. and J. B. Weaver, ``Contrast Enhancement of Medical Images Using Multiscale Edge Representation", SPIE vol. 2242 Wavelet Applications, pp. 711-719, 1994.

[12] http://s20c.smb.man.ac.uk/services/MIAS/MIAScom.html.